View Article Online / Journal Homepage / Table of Contents for this issue
Dynamic Article Links

Journal of Materials Chemistry

Cite this: J. Mater. Chem., 2012, 22, 14149

www.rsc.org/materials

PAPER

Wall-number selective growth of vertically aligned carbon nanotubes from FePt catalysts: a comparative study with Fe catalysts†

Shisheng Li, Pengxiang Hou, Chang Liu,* Libo Gao, Bilu Liu, Lili Zhang, Man Song and Hui-Ming Cheng

Received 12th April 2012, Accepted 17th May 2012
DOI: 10.1039/c2jm32270f

Published on 18 May 2012 on http://pubs.rsc.org | doi:10.1039/C2JM32270F
Downloaded by National University of Singapore on 22/04/2013 08:06:07.

By comparing the Ostwald ripening behavior of FePt and Fe catalyst films on Al_2O_3 substrates, we found that the interaction between FePt and Al_2O_3 is much stronger than that of Fe–Al_2O_3. The strong catalyst–substrate interaction guarantees the formation of high area-density, ultrafine and uniform FePt nanoparticles even at elevated temperatures. When used as the catalyst for growing vertically aligned carbon nanotubes (CNTs), the FePt catalyst produced CNTs with good alignment, narrow diameter distribution, and desirable wall-number selectivity. Characterization showed that the vertically aligned single-walled and double-walled CNTs grown from the FePt catalyst possess high purity, good homogeneity, and superior thermal stability. The catalytic mechanism of the FePt binary catalyst is discussed in comparison with that of the pure Fe catalyst.

Introduction

Carbon nanotubes (CNTs), especially, single-walled CNTs (SWCNTs) and double-walled CNTs (DWCNTs) have received intense research interest due to their unique tubular structure, high specific surface area,[1] and superior mechanical,[2,3] electrical,[4,5] and thermal properties.[6] These structural characteristics and advanced properties make CNTs promising for applications in high performance super-fibers,[2,7] transparent conducting films,[8,9] transistors[10–12] and energy storage and conversion devices.[13] Vertically aligned CNTs (VA-CNTs) are CNT arrays grown perpendicular to a substrate. VA-CNTs show advantages of ordered structure, anisotropic property, and easy manipulation compared with common tangled CNTs. Therefore, VA-CNTs, especially VA-SWCNTs and VA-DWCNTs are considered to be ideal candidates for thermal interface materials,[14] field emitters,[15] and energy and environment-related applications.[16,17] Tremendous effort has been devoted to achieving the controlled synthesis of high purity VA-SWCNTs[18,19] and VA-DWCNTs.[20,21]

According to the well-recognized vapor–liquid–solid growth mechanism, catalyst nanoparticles (NPs) can be viewed as a seed or template for CNT growth[22] and the diameter of the grown CNTs depends strongly on the size of the catalyst NPs. Thus, it is essential to obtain catalyst NPs with desired size, area-density and composition for growing high-quality CNTs with a homogeneous structure, such as wall number, diameter and even bandgap.[23] Controlled fabrication of high area-density, ultrafine catalyst NPs is an important prerequisite for the growth of VA-SWCNTs and VA-DWCNTs. To achieve this objective, the following approaches have been proposed and used: (a) choosing suitable supporting substrates. The interaction between catalyst and substrate plays an important role in the evolution of catalyst NPs at high temperatures. A strong catalyst–substrate interaction will maximize their contact area and reduce the total free energy. Therefore, small catalyst NPs can be stabilized on such a substrate. On the contrary, weak interaction between catalyst and substrate always leads to the fast growth of catalyst NPs. For instance, the interaction of Fe–Al_2O_3 is stronger than that of Fe–SiO_2, thus it is easier to obtain high density Fe NPs on an Al_2O_3 substrate than on SiO_2.[24] (b) Improving the roughness of substrates. By roughening the surface of substrate, the diffusion of the catalyst on it can be effectively restricted thus yielding a high area-density of catalyst NPs with desired size. For example, Fan *et al.*[25] prepared VA-CNTs on a porous silicon substrate. Hata *et al.*[18,20] and Nakayama *et al.*[26] synthesized VA-SWCNTs and VA-DWCNTs on Al_2O_3 substrates with a rough surface. (c) Catalyst pretreatment. Oxidation[27] and nitridation[28,29] of catalyst NPs have proved to be effective in obtaining high-quality VA-CNTs. The formation of the metal oxide and nitride may improve their interactions with the substrates, and thus increase the surface diffusion barrier and alleviate the agglomeration of catalyst NPs.[24] (d) Water enhanced super growth. By introducing weak oxidant H_2O, the super growth of VA-SWCNTs was achieved by Hata *et al.*[18] The function of H_2O was later verified to be that it was able to inhibit the Ostwald ripening, because the introduced oxygen and hydroxyl species can slow down the diffusion of the metal catalyst.[30]

Shenyang National Laboratory for Materials Science, Institute of Metal Research, Chinese Academy of Sciences, Shenyang 110016, P.R. China. E-mail: cliu@imr.ac.cn

† Electronic supplementary information (ESI) available: High resolution TEM image of an FePt NP and the selected area electron diffraction pattern of the FePt NPs. AFM images of FePt and Fe NPs after thermal annealing. Laser Raman and XPS spectra of the grown CNTs. Statistical results of the FePt and Fe NPs. See DOI: 10.1039/c2jm32270f

Published on 18 May 2012 on http://pubs.rsc.org | doi:10.1039/C2JM32270F
Downloaded by National University of Singapore on 22/04/2013 08:06:07.

By choosing suitable substrates with a rough surface and performing suitable catalyst pretreatment, notable progress has been made on the synthesis of VA-CNTs. However, there are still some problems that need to be solved, such as the difficulty in obtaining uniform and ultrafine catalyst NPs.[30] The Fe catalyst NPs tend to diffuse into the substrate at high temperatures and it is also easy for the Fe catalyst NPs to detach from the substrate and become encapsulated in the CNTs.[31] Fe is the most commonly used catalyst for growing VA-CNTs owing to its high catalytic efficiency.[18,20,25] Recently, bimetallic catalysts have been developed and shown advantages in growing VA-CNTs. An FeMo catalyst was found to be effective for the selective growth of VA-SWCNTs.[32] Some other bimetallic catalysts, FeRu,[33] FeNi,[34] FeCu,[35] and CoMo[36] showed great promise in growing SWCNTs with specific chiralities. Therefore, the exploration of effective bimetallic catalysts will benefit the growth of VA-SWCNTs with controlled structure and properties.

FePt NPs with a chemically ordered crystalline phase are promising candidates for ultrahigh area-density magnetic recording media.[37] Due to their unique structure and physical properties, sophisticated methods have been developed to fabricate FePt NPs, such as chemical synthesis[38,39] and sputtering.[40] Recently, FePt NPs were used by Choi *et al.* to grow vertically aligned multi-walled CNTs (VA-MWCNTs).[41] Schaffel *et al.*[42] prepared hard magnetic FePt NP-terminated MWCNTs and pointed out that such a hybrid structure may facilitate the assembly of CNTs and extend their applications.

In this study, we achieve selective synthesis of VA-SWCNTs and VA-DWCNTs by using FePt catalyst films with different thicknesses as the catalyst. Owing to the strong FePt–Al_2O_3 interaction, uniform FePt NPs with high area-density and controlled particle size are stably anchored onto the substrate. As a result, well-aligned, high-quality VA-SWCNTs and VA-DWCNTs were selectively prepared by simple thermal CVD. In addition, the function and growth mechanism produced by the FePt and Fe catalysts were studied and compared.

Experimental

Catalyst deposition

Silicon substrates with a 500 nm thick oxide layer were used as growth substrates. 1 or 2 nm FePt–20 nm Al_2O_3 and 1 or 2 nm Fe–20 nm Al_2O_3 catalyst films were sequentially deposited by ion-beam assisted deposition. For catalyst deposition, a deposition rate of 0.02 nm s^{-1} was used to precisely control the catalyst film thickness, which guarantees the repeatability of the VA-CNT growth. In the case of the FePt catalyst, Fe and Pt films with the same thickness were deposited. The deposition sequence of the Fe and Pt films does not greatly affect the growth of VA-CNTs.

TEM characterization of FePt and Fe NPs

A 50 nm thick Al_2O_3 supporting layer was first deposited onto NaCl crystals, followed by the FePt and Fe catalyst films. The catalyst films were thermally annealed under an Ar–H_2 atmosphere at 775 °C for 10 min, and then cooled to room temperature. After the NaCl crystals were dissolved in water, copper grids were used to fish out the FePt–Al_2O_3 and Fe–Al_2O_3 films.

VA-CNT growth

The VA-CNT growth was conducted in a quartz tube furnace with 25 mm inner diameter. When the furnace temperature was increased to the VA-CNT growth temperature, the quartz chamber was evacuated, then Ar–H_2 mixed gas was introduced to restore the chamber pressure to atmospheric pressure. After that, the growth substrate was pushed into the reaction zone for 10 min thermal annealing. Then C_2H_4 was introduced to initiate the growth of VA-CNTs. The growth was terminated by turning off the C_2H_4 supply and the furnace was cooled in an Ar–H_2 flow. We have studied and compared the growth of VA-CNTs grown from FePt and Fe catalyst over a wide temperature and gas-feeding range and concluded that the FePt catalyst performs better than the pure Fe catalyst. The optimal window for Fe–VA-CNT growth is very narrow (770–780 °C and 200/100/60 sccm Ar/H_2/C_2H_4). However, the optimal growth window for FePt–VA-CNTs is much wider (775–825 °C and 200/100/40–25 sccm Ar/H_2/C_2H_4), which indicates that it is much easier to grow VA-CNTs efficiently from FePt than from the Fe catalyst. To ensure a fair comparison, all the VA-CNTs presented in our manuscript were actually grown at 775 °C and 200/100/60 sccm Ar/H_2/C_2H_4, the optimum growth condition for the Fe catalyst.

Characterization of the catalyst NPs and VA-CNTs

The catalyst NPs were characterized by atomic force microscopy (AFM, multimode NanoScope IIIa, Vecco, operated in the tapping mode), transmission electron microscopy (TEM, JOEL 2010, operated at 200 kV) and X-ray photoelectron spectroscopy (XPS, Escalab 250, Al Kα). The grown VA-CNTs were characterized by scanning electron microscopy (SEM, Nova NanoSEM 430, 15 kV), Raman spectroscopy (Jobin Yvon HR800, excited by 632.8 nm He–Ne laser with laser spot size of ~1 μm^2), XPS and TEM (Tecnai F20, operated at 200 kV). The thermal stability of the VA-CNTs was checked by means of a thermogravimetric analysis (TGA) (NETZSCH STA 449C). TGA experiments were performed with a 50 sccm air flow at a heating rate of 10 °C min^{-1}.

Results and discussion

To grow VA-CNTs with small diameters, it is important to prepare a high area-density of catalyst NPs with small sizes. Because NPs tend to aggregate to form larger ones at elevated temperatures, selecting an appropriate catalyst with slow diffusion rate on the substrate surface is critical. In the case that the metal catalyst has a strong interaction with the substrate, a high area-density of uniform, small NPs can be obtained after thermal annealing (as shown in Fig. 1b). In contrast, when the catalyst has a weak interaction with the substrate, fast growth occurs and a low area-density of non-uniform, large catalyst NPs is ultimately obtained (as shown in Fig. 1d). In this study, we propose to selectively grow high-purity VA-SWCNTs and VA-DWCNTs using a FePt bimetallic catalyst. To compare the thermal aggregation of FePt and Fe catalysts, we deposited FePt and Fe catalyst films with the same thickness. Both of the catalyst films were then annealed under Ar–H_2 atmosphere at 775 °C as illustrated in Fig. 1.

 This journal is © The Royal Society of Chemistry 2012

Published on 18 May 2012 on http://pubs.rsc.org | doi:10.1039/C2JM32270F
Downloaded by National University of Singapore on 22/04/2013 08:06:07.

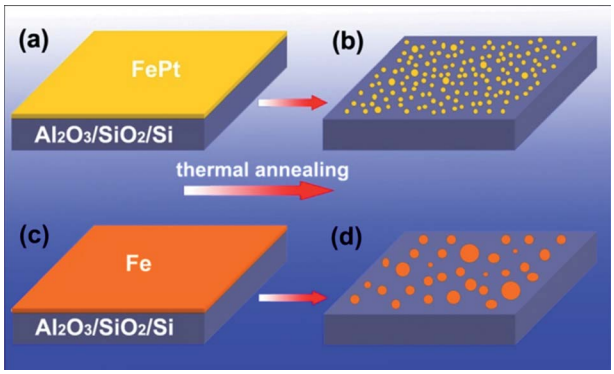


Fig. 1 Schematic of the thermal aggregation of FePt and Fe catalyst films with the same initial thickness.

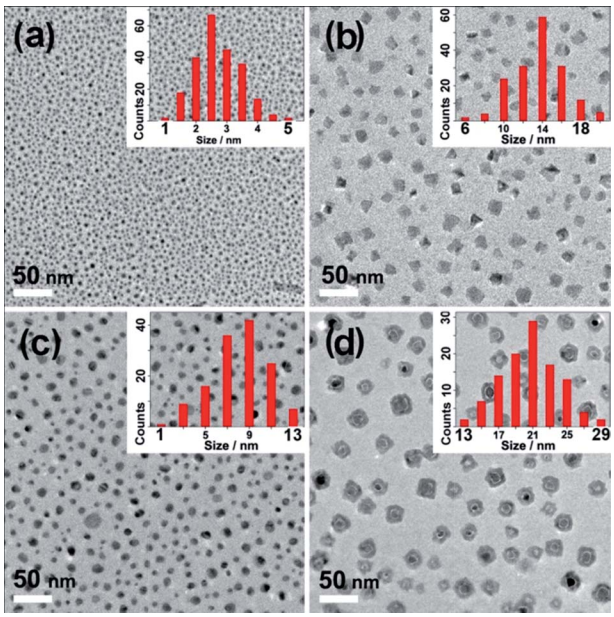


Fig. 2 TEM images of the (a and c) FePt and (b and d) FeO_x catalyst NPs derived from 1 nm (a and b) and 2 nm (c and d) thick catalyst films after annealing under Ar–H_2 atmosphere at 775 °C for 10 min. The insets show the statistical size distribution of the catalyst NPs.

Fig. 2 shows typical TEM images of the FePt (Fig. 2a and c) and Fe (Fig. 2b and d) catalyst NPs derived from 1 nm (Fig. 2a and b) and 2 nm (Fig. 2c and d) thick films after annealing under an Ar–H_2 atmosphere at 775 °C for 10 min. We carefully analysed ~50 catalyst NPs, the high resolution TEM images show that all the FePt NPs are in the alloy state with a face-centred tetragonal (fct) structure. Fig. S1 (ESI†) shows the TEM image of a typical FePt NPs and the selected area electron diffraction pattern of the FePt NPs also well match fct-FePt. The Fe NPs tend to be oxidized when exposed to air–H_2O (Fig. 2b), and Fe–FeO_x core–shell structures were observed (Fig. 2d). Although the FePt and Fe catalyst films are of the same initial thickness, a higher area-density of FePt NPs is obtained that are obviously smaller and more uniform than the corresponding Fe NPs. Furthermore, the FePt NPs are round, quite different from the polygonal FeO_x NPs and irregularly shaped Fe–FeO_x NPs, indicating that no obvious oxidation occurs for the FePt NPs. The mean size of the FePt NPs derived from the 1 nm thick film is 2.7 nm, ~4 times smaller than that of Fe NPs obtained under identical conditions. Moreover, the sizes of the FePt NPs are distributed in the range of 1–5 nm, much narrower than that of Fe NPs (5–17 nm, estimated from the sizes of FeO_x NPs). The area-density of the FePt NPs is ~2.1×10^{12} cm^{-2}, approximately 20 times higher than that of Fe NPs. This can be attributed to the introduction of Pt, which provides more heterogeneous nucleation sites for the FePt NPs. (The detailed size and area-density of the FePt and Fe NPs are listed in Table S1, ESI†.) The FePt NPs obtained show a much smaller mean size and higher area-density than the previously reported Fe NPs for the super growth of a SWCNT forest.[30] These catalyst NPs may facilitate the growth of high-quality VA-CNTs. Compared with the NPs obtained from the 1 nm thick films, TEM and AFM (Fig. S2, ESI†) characterization shows that the catalyst NPs derived from the 2 nm thick films have a larger size and wider size distribution. It is worth noting that the FePt NPs derived from the 2 nm thick FePt catalyst film have a smaller size, a narrower size distribution and are more numerous than the Fe NPs from the 1 nm thick Fe catalyst film, indicating a dramatic NP size restriction effect due to the addition of Pt.

SEM images of VA-CNTs grown from the FePt and Fe catalyst are shown in Fig. 3. It can be seen that the VA-CNTs grown from FePt catalyst are straight and well-aligned (Fig. 3a and c), while the Fe-catalyzed VA-CNTs are much more curved and tangled (Fig. 3b and d). For both FePt and Fe catalysts, increasing catalyst film thickness will lead to a lower density of the grown VA-CNTs. Moreover, the quality of VA-CNTs always has a strong correlation with the CNT alignment. Perfectly aligned CNTs usually have a lower density of defects in their tube walls than curved VA-CNTs.[43] The growth rate of VA-CNTs from the FePt catalyst was found to be slower than that from the Fe catalyst. For example, the heights of the VA-CNTs grown

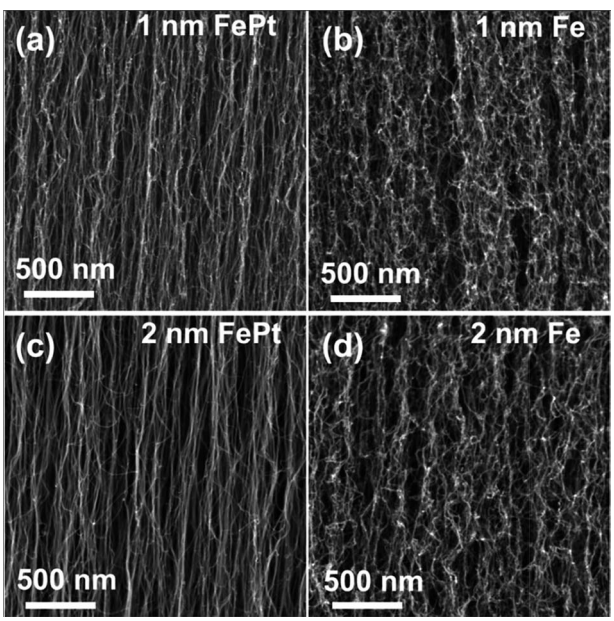


Fig. 3 SEM images of the as-grown VA-CNTs from (a) 1 nm FePt; (b) 1 nm Fe; (c) 2 nm FePt and (d) 2 nm Fe.

Published on 18 May 2012 on http://pubs.rsc.org | doi:10.1039/C2JM32270F
Downloaded by National University of Singapore on 22/04/2013 08:06:07.

from 1 nm FePt, 1 nm Fe, 2 nm FePt, and 2 nm Fe catalysts for 10 minutes were about 50 μm, 270 μm, 300 μm, and 350 μm, respectively. The difference in growth velocity can be attributed to the different solubility and diffusion and precipitation kinetics of the FePt and Fe catalysts.

Our TEM observation and laser Raman spectra as shown in Fig. 4 and Fig. S3 (ESI†) indicate that the CNTs grown from the FePt catalyst have better crystallinity and higher I_G/I_D ratio than those grown from the Fe catalyst. Fig. 4a–d show typical TEM images of the VA-CNTs grown from the 1 or 2 nm thick FePt and Fe catalyst films. It can be seen that the CNTs grown from the FePt catalyst are relatively straight, while the walls of the CNTs grown from the Fe catalyst are usually wavy. In addition, the CNTs grown from FePt catalyst have good wall-number selectivity (Fig. 4e). A SWCNT content of 80.0% and total SWCNT and DWCNT content of 98.0% are obtained for the VA-CNTs grown from the 1 nm thick FePt catalyst film. When the thickness of the FePt catalyst film is increased to 2 nm, a DWCNT content of 70.3% is achieved, and the rest are mainly SWCNTs and triple-walled CNTs. On the other hand, the CNTs grown from Fe NPs show poorer selectivity in wall number, and their wall numbers are in the range of 1–5 layers. The diameter distributions of the CNTs grown from FePt and Fe catalysts are shown in Fig. 4f. The mean diameters of the CNTs grown from the 1 nm FePt, 2 nm FePt, 1 nm Fe, and 2 nm Fe catalyst films are 3.5, 6.5, 7.2, and 8.7 nm, respectively. The mean diameter of the CNTs grown from the 1 nm FePt catalyst film is larger than the mean size of the corresponding FePt NPs, which indicates that some of the very small FePt NPs may be not active for the growth of CNTs. In contrast, the mean diameter of the CNTs grown from the Fe catalyst is always smaller than the mean size of the corresponding Fe NPs. There are two possible reasons accounting for this phenomenon. Firstly, the observed NPs are FeO_x NPs rather than pure Fe NPs,[44] and the FeO_x NPs will be reduced to smaller Fe NPs before CNT growth. Secondly, previous work by Hata *et al.*[45] showed that only 84% of Fe NPs was activated for growing VA-CNTs in a water assisted "supergrowth" process. In this work, there may be also some big Fe NPs that are not activated and do not contribute to the CNT growth.

To characterize the quality and thermal stability of the VA-CNTs, we performed thermal gravimetric analysis (TGA) of the VA-CNTs grown from the 2 nm thick FePt and Fe catalyst films, and the results are shown in Fig. 4g. It can be seen that the VA-CNTs grown from the 2 nm thick FePt catalyst film start to lose weight at ~580 °C (temperature at 5% mass loss), about 80 °C higher than that of the VA-CNTs grown from the 2 nm thick Fe catalyst film. This oxidation temperature is also higher than that of the previously reported water-assisted super growth VA-DWCNTs.[20] The differential scanning calorimetry (DSC) plot of the VA-DWCNTs grown from the 2 nm thick FePt catalyst film have a single narrow exothermic peak at ~725 °C, which indicates high quality and good uniformity of the VA-CNTs. On the other hand, the VA-CNTs grown from the 2 nm thick Fe catalyst film show two wide exothermic peaks at ~590 and 675 °C, indicative of a broad diameter distribution and high defect density.

As discussed above, the catalyst–substrate interaction is of great importance for the growth of VA-CNTs. In this study, the VA-CNTs grown from FePt catalyst are superior in their degree of alignment, wall-number selectivity, diameter distribution, thermal stability, and structural uniformity over the CNTs grown from pure Fe catalyst. We believe that these characteristics can be attributed to the introduction of Pt, which increases the catalyst–substrate interaction, and hence improves the quality and controllability of the grown VA-CNTs. To verify this assumption, the following experiments were designed and conducted to compare the FePt–Al_2O_3 and Fe–Al_2O_3 interactions.

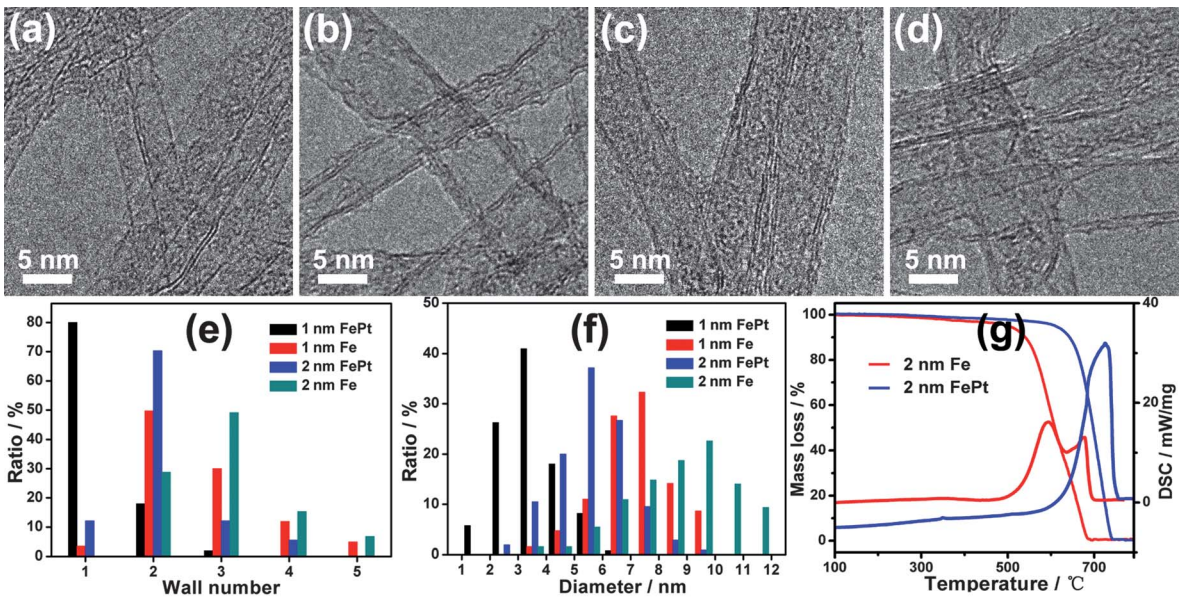


Fig. 4 Typical TEM images of the VA-CNTs grown from (a) 1 nm FePt; (b) 1 nm Fe; (c) 2 nm FePt and (d) 2 nm Fe. (e) Wall-number distribution of the VA-CNTs grown from 1 and 2 nm FePt and Fe. (f) Diameter distribution of the VA-CNTs obtained from 1 and 2 nm FePt and Fe. (g) TG and DSC plots of the VA-CNTs grown from 2 nm FePt and Fe under an air atmosphere.

 This journal is © The Royal Society of Chemistry 2012

Published on 18 May 2012 on http://pubs.rsc.org | doi:10.1039/C2JM32270F
Downloaded by National University of Singapore on 22/04/2013 08:06:07.

We first performed VA-CNT growth using FePt and Fe as the catalyst for 10 min and 60 min, the grown VA-CNTs were then peeled from the substrates with tweezers, and finally an oxygen plasma treatment was performed on the substrates to remove any remaining CNTs. AFM observations of the resulting substrates are shown in Fig. 5. It can be seen that for both 10 min and 60 min growth time, the area-density and uniformity of the FePt NPs are better than those of Fe NPs, indicative of a stronger interaction between FePt and Al_2O_3 than between Fe–Al_2O_3. For the Fe–Al_2O_3 system, the catalyst NPs can be easily lifted from the substrate due to the pulling force originating from the neighbouring CNTs with a different growth velocity and a weak catalyst–substrate interaction. When carbon atoms precipitate from the detached Fe NPs and form a coating layer, the growth of the CNT terminates (Fig. 6a). Therefore, when the growth time was increased from 10 min to 60 min, more Fe NPs were pulled from the Al_2O_3 substrate leaving more holes, as shown in Fig. 5b and d. For the FePt–Al_2O_3 system, there are almost no holes on the substrate (Fig. 5a and c). However, the height of the FePt NPs increased after the prolonged growth procedure. This can be attributed to the Ostwald ripening of the FePt NPs during the VA-CNT growth process.[46]

To investigate the status and fine structure of the FePt NPs, some VA-CNTs were scratched from the substrate with tweezers. The samples were then sonicated and dropped onto a copper grid for TEM observation. The strong sonication treatment often leads to the detachment of CNTs from FePt NPs, while the FePt NPs are still in intimate contact with the Al_2O_3 substrate, showing a strong catalyst–substrate interaction. Fig. 6b shows a typical TEM image of a FePt NP half-embedded in the Al_2O_3 matrix. The FePt NP is of the $L1_0$ phase, and the (200) and (111) lattice fringes are clearly resolved in the $L1_0$ superstructure.

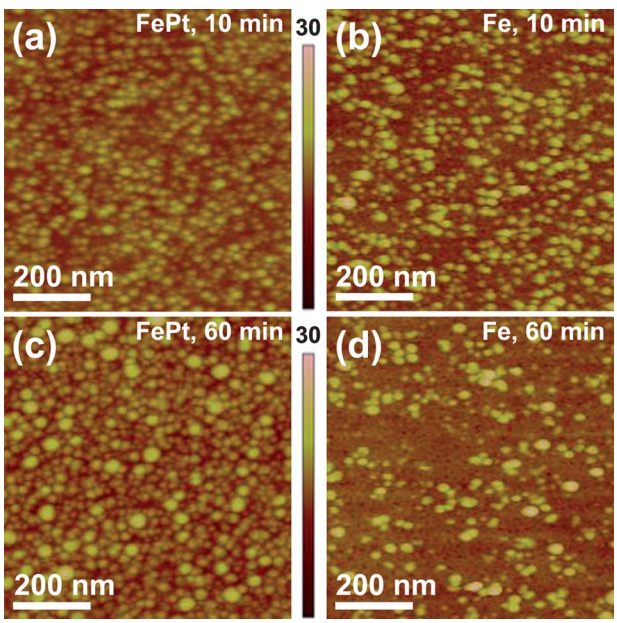


Fig. 5 AFM images of the (a) 2 nm thick FePt after 10 min VA-CNT growth, (b) 2 nm thick Fe after 10 min VA-CNT growth, (c) 2 nm thick FePt after 60 min VA-CNT growth, and (d) 2 nm thick Fe after 60 min VA-CNT growth. The as-grown VA-CNTs were removed by oxygen plasma treatment before the AFM characterization.

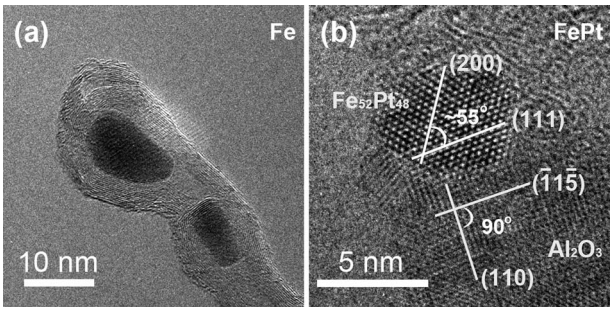


Fig. 6 TEM images of (a) two deactivated Fe NPs encapsulated by carbon shells; (b) a FePt NP half-embedded in the Al_2O_3 matrix.

We further checked the catalyst residues in the VA-CNTs by XPS, and the results are shown in Fig. S4 (ESI†). For different etching depths, no Fe or Pt residues were observed in the VA-CNTs grown from the FePt catalyst. However, in the case of VA-CNTs grown from the Fe catalyst, a trace amount of Fe residue is always detectable irrespective of the etching depth. TEM observation demonstrates that the residual Fe NPs are encapsulated in carbon layers as shown in Fig. 6a. It is difficult to remove such metal residues by simple acid washing due to the protective effect of the graphitic layers.

Besides the strong interaction between FePt and Al_2O_3, another unique feature of the FePt catalyst is that the addition of Pt dramatically improves the C_2H_4 dissociation efficiency and widens the temperature window for VA-CNT growth from 700 °C to 950 °C due to the improved dehydrogenation efficiency[47] and thermal stability.[48] For instance, at 775 °C, the lowest C_2H_4 concentration for the 1 nm Fe catalyst film to grow VA-CNTs is ~10.7%, while the lowest C_2H_4 concentration for the 1 nm FePt catalyst film to grow VA-SWCNTs is only ~1.9%, which implies that the dissociation efficiency of C_2H_4 is dramatically improved for the bimetallic FePt catalyst.

Conclusions

High-quality VA-SWCNTs and VA-DWCNTs are selectively prepared by using FePt catalyst films with different thicknesses. The introduction of Pt increases the catalyst–substrate interaction and the hydrocarbon dissociation ability of the bimetallic catalyst, and hence VA-CNTs with a superior degree of alignment, wall-number selectivity, thermal stability, and purity are obtained. Due to the strong catalyst–substrate interaction, almost no residual metal catalyst can be detected in the harvested VA-CNTs. Further optimization on the composition, size, and structure of the FePt catalyst as well as the CVD growth conditions may facilitate the better controlled growth of VA-CNTs with a specific wall number, diameter, and even electrical properties.

Acknowledgements

This work was supported by the Ministry of Science and Technology of China (Grants 2011CB932601, 2011CB932604, and 2008DFA51400) and National Natural Science Foundation of China (Grants 50921004 and 50872137).

View Article Online

Notes and references

1 T. Hiraoka, A. Izadi-Najafabadi, T. Yamada, D. N. Futaba, S. Yasuda, O. Tanaike, H. Hatori, M. Yumura, S. Iijima and K. Hata, *Adv. Funct. Mater.*, 2010, **20**, 422.
2 F. Li, H. M. Cheng, S. Bai, G. Su and M. S. Dresselhaus, *Appl. Phys. Lett.*, 2000, **77**, 3161.
3 Y. J. Li, K. L. Wang, J. Q. Wei, Z. Y. Gu, Z. C. Wang, J. B. Luo and D. H. Wu, *Carbon*, 2005, **43**, 31.
4 Z. Yao, C. L. Kane and C. Dekker, *Phys. Rev. Lett.*, 2000, **84**, 2941.
5 A. A. Green and M. C. Hersam, *Nat. Nanotechnol.*, 2009, **4**, 64.
6 P. Kim, L. Shi, A. Majumdar and P. L. McEuen, *Phys. Rev. Lett.*, 2001, **87**, 215502.
7 A. B. Dalton, S. Collins, E. Munoz, J. M. Razal, V. H. Ebron, J. P. Ferraris, J. N. Coleman, B. G. Kim and R. H. Baughman, *Nature*, 2003, **423**, 703.
8 Z. C. Wu, Z. H. Chen, X. Du, J. M. Logan, J. Sippel, M. Nikolou, K. Kamaras, J. R. Reynolds, D. B. Tanner, A. F. Hebard and A. G. Rinzler, *Science*, 2004, **305**, 1273.
9 R. K. Jackson, A. Munro, K. Nebesny, N. Armstrong and S. Graham, *ACS Nano*, 2010, **4**, 1377.
10 A. Javey, H. Kim, M. Brink, Q. Wang, A. Ural, J. Guo, P. McIntyre, P. McEuen, M. Lundstrom and H. J. Dai, *Nat. Mater.*, 2002, **1**, 241.
11 Y. X. Zhou, A. Gaur, S. H. Hur, C. Kocabas, M. A. Meitl, M. Shim and J. A. Rogers, *Nano Lett.*, 2004, **4**, 2031.
12 C. Wang, J. L. Zhang, K. M. Ryu, A. Badmaev, L. G. De Arco and C. W. Zhou, *Nano Lett.*, 2009, **9**, 4285.
13 D. N. Futaba, K. Hata, T. Yamada, T. Hiraoka, Y. Hayamizu, Y. Kakudate, O. Tanaike, H. Hatori, M. Yumura and S. Iijima, *Nat. Mater.*, 2006, **5**, 987.
14 K. Kordas, G. Toth, P. Moilanen, M. Kumpumaki, J. Vahakangas, A. Uusimaki, R. Vajtai and P. M. Ajayan, *Appl. Phys. Lett.*, 2007, **90**, 123105.
15 T. Y. Tsai, C. Y. Lee, N. H. Tai and W. H. Tuan, *Appl. Phys. Lett.*, 2009, **95**, 013107.
16 V. L. Pushparaj, M. M. Shaijumon, A. Kumar, S. Murugesan, L. Ci, R. Vajtai, R. J. Linhardt, O. Nalamasu and P. M. Ajayan, *Proc. Natl. Acad. Sci. U. S. A.*, 2007, **104**, 13574.
17 M. Yu, H. H. Funke, J. L. Falconer and R. D. Noble, *Nano Lett.*, 2009, **9**, 225.
18 K. Hata, D. N. Futaba, K. Mizuno, T. Namai, M. Yumura and S. Iijima, *Science*, 2004, **306**, 1362.
19 L. T. Qu, F. Du and L. M. Dai, *Nano Lett.*, 2008, **8**, 2682.
20 T. Yamada, T. Namai, K. Hata, D. N. Futaba, K. Mizuno, J. Fan, M. Yudasaka, M. Yumura and S. Iijima, *Nat. Nanotechnol.*, 2006, **1**, 131.
21 I. Gunjishima, T. Inoue, S. Yamamuro, K. Sumiyama and A. Okamoto, *Carbon*, 2007, **45**, 1193.
22 K. L. Jiang, C. Feng, K. Liu and S. S. Fan, *J. Nanosci. Nanotechnol.*, 2007, **7**, 1494.
23 W. Song, C. Jeon, Y. S. Kim, Y. T. Kwon, D. S. Jung, S. W. Jang, W. C. Choi, J. S. Park, R. Saito and C. Y. Park, *ACS Nano*, 2010, **4**, 1012.
24 C. Mattevi, C. T. Wirth, S. Hofmann, R. Blume, M. Cantoro, C. Ducati, C. Cepek, A. Knop-Gericke, S. Milne, C. Castellarin-Cudia, S. Dolafi, A. Goldoni, R. Schloegl and J. Robertson, *J. Phys. Chem. C*, 2008, **112**, 12207.
25 S. S. Fan, M. G. Chapline, N. R. Franklin, T. W. Tombler, A. M. Cassell and H. J. Dai, *Science*, 1999, **283**, 512.
26 S. Chakrabarti, H. Kume, L. J. Pan, T. Nagasaka and Y. Nakayama, *J. Phys. Chem. C*, 2007, **111**, 1929.
27 H. Sato, Y. Hori, K. Hata, K. Seko, H. Nakahara and Y. Saito, *J. Appl. Phys.*, 2006, **100**, 104321.
28 K. M. Choi, S. Augustine, J. H. Choi, J. H. Lee, W. H. Shin, S. H. Yang, J. Y. Lee and J. K. Kang, *Angew. Chem., Int. Ed.*, 2008, **47**, 9904.
29 D. H. Lee, W. J. Lee and S. O. Kim, *Nano Lett.*, 2009, **9**, 1427.
30 P. B. Amama, C. L. Pint, L. McJilton, S. M. Kim, E. A. Stach, P. T. Murray, R. H. Hauge and B. Maruyama, *Nano Lett.*, 2009, **9**, 44.
31 K. Liu, K. L. Jiang, Y. Wei, S. P. Ge, P. Liu and S. S. Fan, *Adv. Mater.*, 2007, **19**, 975.
32 H. Nishino, S. Yasuda, T. Namai, D. N. Futaba, T. Yamada, M. Yumura, S. Iijima and K. Hata, *J. Phys. Chem. C*, 2007, **111**, 17961.
33 X. L. Li, X. M. Tu, S. Zaric, K. Welsher, W. S. Seo, W. Zhao and H. J. Dai, *J. Am. Chem. Soc.*, 2007, **129**, 15770.
34 W. H. Chiang and R. M. Sankaran, *Nat. Mater.*, 2009, **8**, 882.
35 M. He, A. I. Chernov, P. V. Fedotov, E. D. Obraztsova, J. Sainio, E. Rikkinen, H. Jiang, Z. Zhu, Y. Tian, E. I. Kauppinen, M. Niemela and A. O. I. Krauset, *J. Am. Chem. Soc.*, 2010, **132**, 13994.
36 S. M. Bachilo, L. Balzano, J. E. Herrera, F. Pompeo, D. E. Resasco and R. B. Weisman, *J. Am. Chem. Soc.*, 2003, **125**, 11186.
37 Y. F. Xu, M. L. Yan and D. J. Sellmyer, *J. Nanosci. Nanotechnol.*, 2007, **7**, 206.
38 S. H. Sun, C. B. Murray, D. Weller, L. Folks and A. Moser, *Science*, 2000, **287**, 1989.
39 C. Liu, X. W. Wu, T. Klemmer, N. Shukla, X. M. Yang, D. Weller, A. G. Roy, M. Tanase and D. Laughlin, *J. Phys. Chem. B*, 2004, **108**, 6121.
40 M. Watanabe, T. Masumoto, D. H. Ping and K. Hono, *Appl. Phys. Lett.*, 2000, **76**, 3971.
41 B. H. Choi, Y. M. Kim, Y. B. Kim, J. H. Lee and D. C. Shin, *J. Nanosci. Nanotechnol.*, 2010, **10**, 3543.
42 F. Schaffel, C. Taschner, M. H. Rummeli, V. Neu, U. Wolff, U. Queitsch, D. Pohl, R. Kaltofen, A. Leonhardt, B. Rellinghaus, B. Buchner and L. Schultz, *Appl. Phys. Lett.*, 2009, **94**, 193107.
43 Y. Y. Zhang, G. F. Zou, S. K. Doorn, H. Htoon, L. Stan, M. E. Hawley, C. J. Sheehan, Y. T. Zhu and Q. X. Jia, *ACS Nano*, 2009, **3**, 2157.
44 C. M. Wang, D. R. Baer, J. E. Amonette, M. H. Engelhard, J. Antony and Y. Qiang, *J. Am. Chem. Soc.*, 2009, **131**, 8824.
45 D. N. Futaba, K. Hata, T. Namai, T. Yamada, K. Mizuno, Y. Hayamizu, M. Yumura and S. Iijima, *J. Phys. Chem. B*, 2006, **110**, 8035.
46 A. Borjesson and K. Bolton, *ACS Nano*, 2011, **5**, 771.
47 A. P. Barkova, D. B. Furman and V. B. Kazansky, *Kinet. Catal.*, 1996, **37**, 591.
48 Y. K. Takahashi, M. Ohnuma and K. Hono, *J. Appl. Phys.*, 2003, **93**, 7580.

Published on 18 May 2012 on http://pubs.rsc.org | doi:10.1039/C2JM32270F
Downloaded by National University of Singapore on 22/04/2013 08:06:07.

This journal is © The Royal Society of Chemistry 2012